Biophysical Chemistry 276 (2021) 106627

Contents lists available at ScienceDirect

Biophysical Chemistry

journal homepage: www.elsevier.com/locate/biophyschem

How procyanidin C1 sticks to collagen: The role of proline rings

André Nicolai Petelski [a,b,*], Silvana Carina Pamies [a,*], Gladis Laura Sosa [a,b]

[a] Grupo de Investigación en Química Teórica y Experimental (QUITEX), Departamento de Ingeniería Química, Universidad Tecnológica Nacional, Facultad Regional Resistencia, French 414 (H3500CHJ), Resistencia, Chaco, Argentina
[b] Instituto de Química Básica y Aplicada del Nordeste Argentino, IQUIBA-NEA, UNNE-CONICET, Avenida Libertad 5460, 3400 Corrientes, Argentina

ARTICLE INFO

Keywords:
Hydrogen bonds
Stacking
Proline
Polyphenol
Protein

ABSTRACT

Molecular interactions between proteins and polyphenols are responsible for many natural phenomena like colloidal turbidity, astringency, denaturation of enzymes and leather tanning. Although these phenomena are well known, there are open questions about the specific interactions involved in the complexation process. In this work, Molecular Dynamic (MD) simulations and the topology of the electron density analysis were used to study the interactions between the flavonoid procyanidin C1 and a collagen fragment solvated in water. Root mean square deviation; root mean square fluctuation and hydrogen bonds occupancy were examined after 50 ns. The interactions were also analyzed by means of the quantum theory of atoms in molecules. Our results show that the main interactions are hydrogen bonds between –OH groups of the polyphenol and C═O groups of the peptide bond. Stacking interactions between proline rings and phenol rings, that is C—H···π hydrogen bonds, also stabilize the dynamic structure of the complex.

1. Introduction

Interactions between proteins and polyphenols have been subject of several researches in the last decade. [1–3] Their numerous biological effects, like antioxidant, [4,5] anticarcinogenic, [6,7] antiviral, [8] antiallergic [9] and anti-inflammatory properties, [10,11] are well documented in the literature.

In the technological process of beverages production, proteins and polyphenols, when they are combined, are the main precursors of the undesirable phenomenon of colloidal turbidity. [12] The visible haze not only causes unpleasant organoleptic sensations, but it also shortens the shell life of beverages [13–15] Siebert et al. [16] have suggested a binding model in which protein chains are interconnected with each other through polyphenolic compounds. Polyphenols and proteins are thus bound through hydrogen bonds (HB), and mainly hydrophobic bindings, [17,18] in sites where the amino acid proline (Pro) is located. Additionally, it has been stated that polyphenols have more affinity to proteins with a high molar ratios of Pro [19] than polypeptides lacking this amino acid. [20] This phenomenon may be attributed to the fact that Pro residues promote the exposure of the backbone and thus the carbonyl groups are also exposed for hydrogen bonding.

The protein-polyphenols interactions are also present in the tanning processes of the leather industry: a polyphenol mixture derived from the collagen of skin, which interacts with synthetic or natural tannins of different sources like wood, roots or leaves. Then, after different refining processes, the skin is turned into leather. [21,22] In a model system formed by a fragment of a collagen triple helix solvated in a mixed solvent of water/gallic acid, Bronco et al. [23] have shown that the backbone protein is more stabilized in a mixed solvent than in pure water. They have also concluded that gallic acid binds with higher affinity to Pro and Hyp residues. [23,24]

Polyphenols also have a demonstrated inhibitory effect on the catalytic activity of enzymes. [25,26] Once inside the pocket, the mechanism of binding includes two leading interactions: hydrogen bonds between hydroxyl groups and electron donating groups, and stacking interactions (hydrophobic) between polyphenol rings and aromatic residues like phenylalanine and tyrosine. [27,28]

On the other hand, the phenomenon known as astringency is due to the interactions between Pro-rich salivary proteins and polyphenols from beverages like wine and tea. [2,29–31] Through NMR titration experiments, Baxter et al. [32] have demonstrated that two adjacent Pro residues are preferred binding sites over single ones. In addition, their proposed model suggests face-to-face interactions between galloyl rings and the Pro residues of the proline-rich peptide. Charlton et al. [33] have

* Corresponding authors at: Grupo de Investigación en Química Teórica y Experimental (QUITEX), Departamento de Ingeniería Química, Universidad Tecnológica Nacional, Facultad Regional Resistencia, French 414 (H3500CHJ), Resistencia, Chaco, Argentina.
E-mail addresses: npetelski@frre.utn.edu.ar (A.N. Petelski), scpamies@frre.utn.edu.ar, sc.pamies@gmail.com (S.C. Pamies), glsosa@frre.utn.edu.ar (G.L. Sosa).

https://doi.org/10.1016/j.bpc.2021.106627
Received 23 February 2021; Received in revised form 7 May 2021; Accepted 25 May 2021
Available online 29 May 2021

also observed face-to-face stacking between epigallocatechin gallate and Pro rings. On the contrary, in their model composed by procyanidin B3 and the human salivary protein fragment $IB7_{14}$ (SPPGKPQGPPPQGG), Simon et al. [34] have not observed stacking interactions between Pro and phenolic rings, which seems to disagree with the previous discussed studies. In a recent work, we have computationally demonstrated how catechin and procyanidin B3 interact with an artificial pentapeptide of proline. [18] However, it is still unknown whether the same interactions will persist within a more realistic protein model.

According to experimental evidence and simulations, interactions between proteins and polyphenols have not yet been fully described at a molecular level. Thus, in order to contribute to the comprehension of the mechanism by means of which polyphenols bind to proteins, in this work, we have combined molecular dynamic (MD) simulations with an electronic structure method. A model structure of a complex formed by a collagen-like peptide (PDB ID A189) as a haze-active protein, and the flavonoid procyanidin C1 (PC1) as a haze-active polyphenol were selected; the system was then solvated in water. The mechanism of complex formation has been examined by means of MD simulations and the interactions involved were studied in the framework of Bader's [35] quantum theory of atoms in molecules (QTAIM).

2. Computational details

2.1. Haze-active polyphenol model

Procyanidin C1 (PC1) is the main trimer found in several foods like cocoa, cinnamon, tea, and fruits like apple, litchi, grape, peach, and berries. [36] Besides, Procyanidin C2 is found in fermented beverages like beer. [37] The PC1 molecule (Fig. 1**)** was built and optimized at the B3LYP/6-31G* level of theory using the Gaussian 03 suit of programs. [38] The atomic charges were calculated with the RESP method [39] using the Gaussian03 [38] suit of programs.

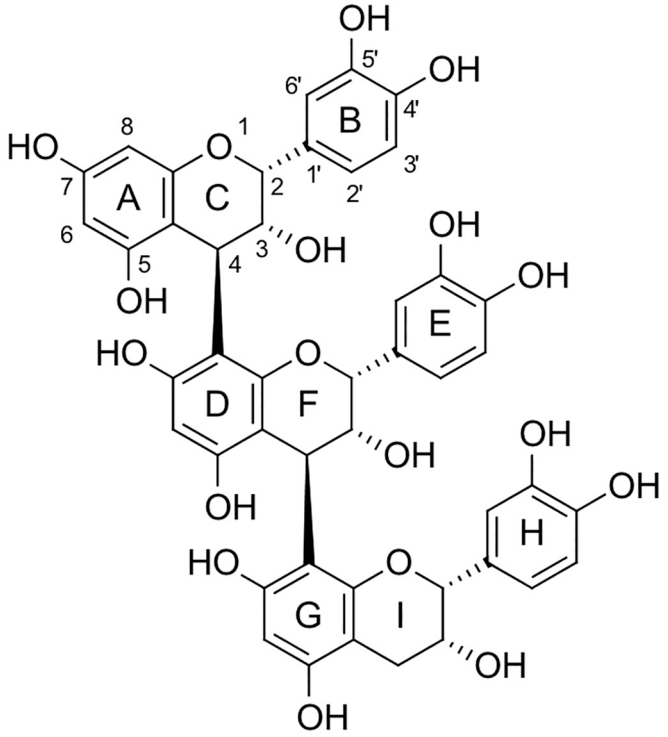

Fig. 1. Molecular Structure of Procyanidin C1.

2.2. Haze-active protein model

Models of collagen structures have the $[XxxYyyGly]_n$ motif. A short segment of 7 amino acids G-(KPG)-(PRG) was extracted from a synthetic peptide of Ruggiero et al. [40] as shown in Fig. 2, with both neutral terminal groups (C-terminal carboxylate and N-terminal amine group). This structure was originally deposited in the PDB Archive (PDBid 1A89) and now is deposited in the Modelarchive. Despite the $[ProHypGly]_n$ or $[ProProGly]_n$ motifs are predominantly found in nature, [41] some of the sequences of our model can be found in other polypeptides of interest. For instance, the $(PRG)_{10}$ structure have formed collagen-like triple helix structures with other polypeptides. [42] Furthermore the (PRG) and (KPG) sequences are also found in bovine type I collagen microfibril. [43] The (GKP) unit can also be found in the human salivary protein fragment IB7 (SPPGKPQGPPPQGG). [34] In addition, the -P-G-P- sequence will be present in collagen polypeptides with the $(PPG)_n$ motif. We did not include the Hyp reside because it was demonstrated by Siebert et al. [16] that synthetic polymers of this amino acid do not form haze at any concentration. Therefore, we think our selected model is a good representation of several haze active environments.

2.3. Molecular dynamic simulations

The PC1 and the PP molecules were randomly placed at a considerable distance to avoid any interaction. The positively charged system was neutralized by adding two Cl^- charge-balancing counterions. The system was then solvated in a truncated octahedral box with 1710 TIP3P [44] water molecules. The same fragment of collagen was also simulated in pure water in a truncated octahedral box with 1465 TIP3P [44] water molecules.

Molecular dynamic simulations were carried out with AMBER 11 software [45]. The parametrization was accomplished by adopting the GAFF force field for the PC1 and the ff99SB force field for the PP. All simulations were preceded by 2 steps of an energetic minimization. The first step was performed with harmonic force restraints over the polyphenol and the PP; on the second step the whole system was minimized. The resulting system of minimal potential energy was subjected to a MD of 500 ps under constant volume conditions, to reach a temperature of 300 K with movement restrictions over the PC1 and the collagen

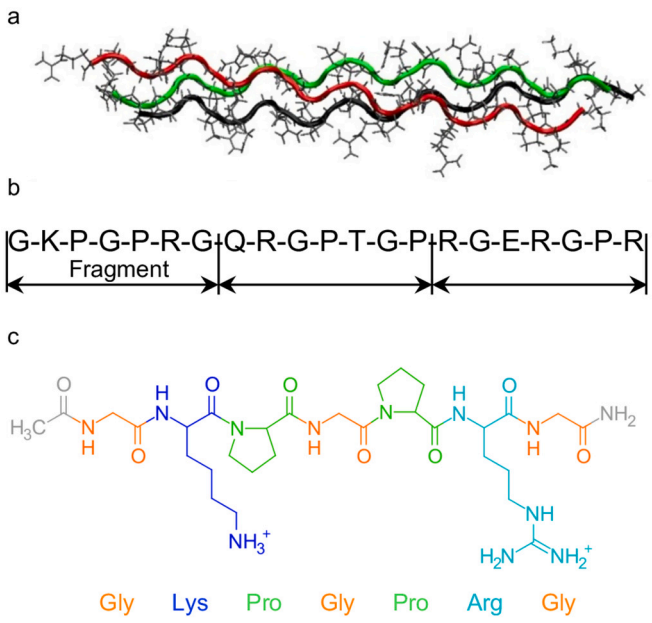

Fig. 2. (a) Molecular structure of Collagen triple-helix (PDB 1A89). (b) Primary structure of a single chain with single-letter amino acid code (c) Molecular structure of the selected fragment = 96 atoms.

fragment. Then, the step was resumed in the NPT ensemble at 300 K and 1 atm of pressure, without restraints over the molecules, during 10 ns to reach the equilibrium over a reasonable density. The constant temperature was maintained in 300 K using the bath coupling algorithm of Langevin [46], and all the bond lengths involving hydrogen atoms were restricted with the SHAKE [47] algorithm. To obtain data, a MD of 50 ns in the NVT ensemble was performed, with a weak-coupling constant of temperature. For long-range interactions the Particle–Mesh Ewald (PME) method was employed, while Van der Wall interactions were evaluated with the Lennard-Jones potential. The cut-off for non-bonded Van der Wall interactions was set at 10 Å. The movement equations were integrated with a simulation step of 2 fs. All of the MD results were analyzed with the PTRAJ module of AMBER 11. [45].

2.4. Topology of the electron density

Molecular interactions were analyzed over a molecular structure taken from the MD runs by a topological analysis of the electron charge density with the QTAIM [35] using the programs AIMAll [48] and MultiWFN [49]. A wave function was obtained with the Hartree Fock (HF) functional and the 6-31G(d) basis set using the Gaussian 09 [38] suit of programs. Despite the HF method does not include electron correlation, and since the results are qualitatively in agreement with those reported by other authors, we could say that calculations at higher levels of theory (B3LYP e.g.) would not significantly change our results although some minor interactions could disappear. Moreover, valuable results about HB have been obtained within this method [18,50]. The graphical presentations of the results obtained were prepared using the VMD program [51].

In order to describe the non-local dispersion interactions, in a more detailed way, reduced model systems were also optimized using the exchange functional developed by Becke [52], the gradient corrected functional of Lee, Yang, and Parr [53] and the DFT-D3(BJ) method developed by Grimme and coworkers [54], which contains the damping function proposed by Becke and Johnson [55] (BLYP-D3(BJ) functional). These calculations were performed with the 6–311++G(d,p) basis set. The interactions were also further analyzed in the framework of the QTAIM at the same level of theory. According to the QTAIM, a bond between two atoms is characterized by a line of maximum electron density, the bond path, that connects the respective nuclei and intersects the zero-flux surface of the electron density gradient field ($\nabla\rho(r_c)$) at a topological (3,−1) critical point, called the bond critical point (BCP). Within this approach, different topological properties evaluated at the BCP were used to characterize interactions: the electron charge density, $\rho(r_c)$, which measures the accumulation of charge between the bonded nuclei and reflects the bond strength [50,56]; the Laplacian of the electron density $\nabla^2\rho(r_c)$, which provides information about the local charge concentration ($\nabla^2\rho(r_c) < 0$) or depletion ($\nabla^2\rho(rc) > 0$); and the densities of potential energy, $V(r_c)$; and the sum of the total energy, H (r_c), which is generally used to analyze the covalent character of the interactions according to Cremer and Kraka [57] criterion.

3. Results and discussion

3.1. Molecular dynamics

3.1.1. Protein conformational mobility

In order to compare the relative stability of the isolated PP in water and in the presence of PC1, root mean square deviations (RMSD) of the PP backbone relative to the initial conformation, as a function of simulation time, were calculated and plotted in Figs. 3a, b. The RMSD of the isolated PP (Fig. 3a) shows big fluctuations that range from an average of 1 to 4 Å suggesting a high flexibility of the backbone. Such conformational changes oscillate during all the simulation, and it seems that they do not have a tendency to reach a stable value. Regarding the system with PC1, the PP backbone oscillates, but it is more stable, with

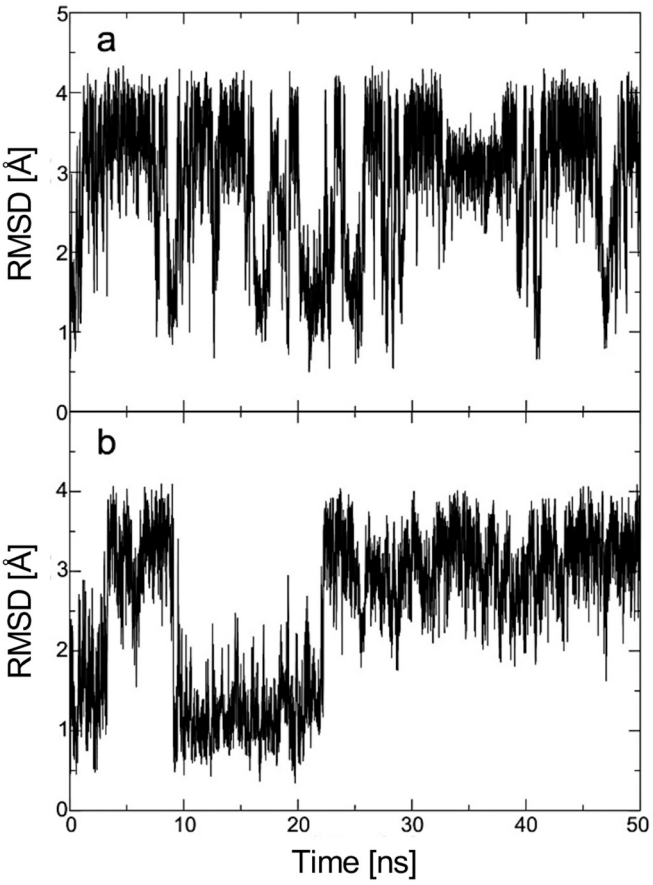

Fig. 3. RMSD time series of backbone atoms (C-Cα-N). (a) Isolated PP in water. (b) Ternary system.

values that range from 2.5 to 3.5 Å at 22.5 ns of the simulation, as can be seen in Fig. 3b. In the last case the PP also shows two main conformational transitions at the beginning of the simulation (0–20 ns) but much less frequently. In line with MD results reported by Bronco and coworkers [23,24], the major changes in the conformation of collagen occur when the PP is in water, with reference to the same fragment in the presence of PC1.

All these results suggest that the PC1 affects the conformational structure of the PP. The structural flexibility was also explored by calculating the average root mean square fluctuation (RMSF) values of the PP backbone (N-Cα-C) throughout the 50 ns of the simulation. In general, it is accepted that after complex formation the conformational mobility of the protein is reduced. This fact is shown in Fig. 4, in which the overall fluctuations of the PP in the complex is lower than that of the isolated one, and the values range from 1 to 9 Å. However, there is an amino acid in the isolated system (Gly) which has lower mobility than the PP in the complex system. Interestingly, there is a concave region in the complex curve (continuous line) that corresponds to Pro, which is in agreement with the findings of Monti et al. [24] for a system of a collagen fragment and mixtures of gallic acid. Interactions that strongly reduce the PP mobility will be shown below.

When analyzing the MD trajectories, it could be observed that a complex with the minimum potential energy occurs at 32.486 ns of the simulation. This structure was extracted from the simulation and then all water molecules were removed (see Fig. 5). An observation of Fig. 5 shows the formation of a complex between both compounds. Despite both molecules were randomly positioned and separated from each other, the PC1 is closely bound to the peptide. Fig. 5 also shows how the PP takes place between two aromatic rings of PC1. It is also observed that the polyphenol surrounds a face of the PP.

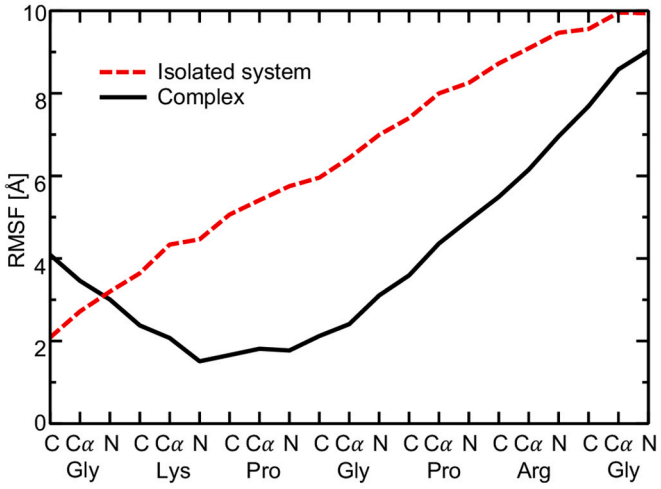

Fig. 4. Root mean square fluctuation of PP backbone atoms.

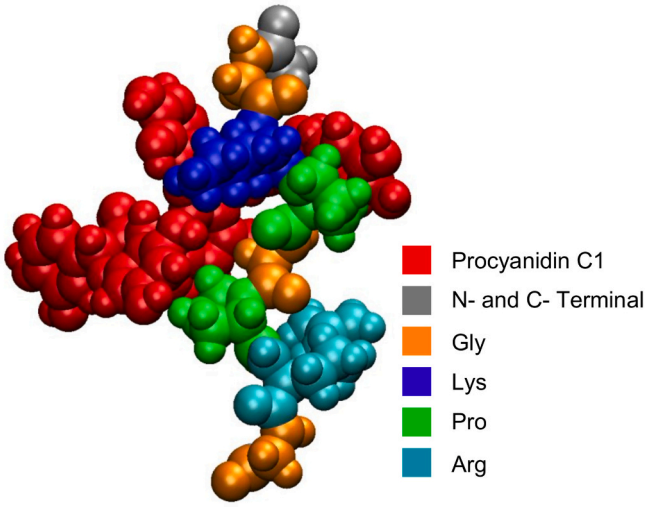

Fig. 5. Snapshot of the minimum potential energy structure.

The backbone dihedral angles defining the conformational flexibility of the peptide are ϕ (C′-N-Ca-C′), ψ (N-Ca-C′-N), and ω (Ca-C′-N-Ca). Table 1 collects the dihedral values of the peptide within the complex of Fig. 5, and those values corresponding to the original PDB structure (values in parentheses). When comparing both angles, one can notice that the amino acids within the (PGP) sequence are the only ones that keep the original values of collagen-like structure. In addition, both Pro residues exhibit similar dihedral values as that in the polyproline type II (PPII) structure ($\phi = -75°$, $\psi = +145°$, $\omega = 180°$). [58] This polypeptide is characterized by an open structure without intramolecular hydrogen bonds. Therefore, the fact that Pro residues take dihedral values close to the ones found in the PPII might explain why the PC1 binds near the (PGP) sequence.

3.1.2. Hydrogen bonds

Polypeptide/PC1, PP/water and PC1/water interactions were analyzed in terms of occupancy percentages over the simulation time. The occupancy percentage is defined as the percentage over the total simulation time in which geometrical criteria are satisfied. The cut-off for geometrical criteria was established in 3.0 Å for the donor-acceptor distance and 120° for the D–H···A angle (D = donor, A = acceptor).

As it can be seen in Table 2A, a small number of HB between the PP and the PC1 is formed, and just one of them is present in almost all the analyzed trajectory. Despite the great number of –OH groups of PC1 (15 –OH groups), the polyphenol binds to the PP just through 3 –OH groups, that is: $–O_{5A}H$, $–O_{7D}H$ and $–O_{3F}H$. Taking into account the number of HB and their percentages of occupancy, the most stable interactions are those with Lys and Pro residues. Distance and angle values are also in good agreement with typical values for HB [59]. These results are consistent with experimental studies of Asano et al. [20] and Siebert et al. [16]. They have shown that the polyphenol binds preferably where the amino acid Pro is present, a key amino acid of the active site. In addition, Bronco et al. [23] have found that even a simple phenolic compound like gallic acid preferably binds to Pro and Hyp.

Table 1
Backbone dihedral angles of the G-(KPG)-(PRG) structure.

Amino acid	One-letter code	ϕ[a]	ψ[b]	ω[c]
Gly	G	58.2 (−66.5)	−170.5 (146.1)	−177.4 (179.7)
Lys	K	−99.8 (−66.5)	168.4 (156.0)	167.7 (−179.8)
Pro	P	−73.9 (−69.7)	151.4 (154.2)	176.1 (179.8)
Gly	G	−62.5 (−70.5)	157.1 (154.2)	−177.7 (179.7)
Pro	P	−72.7 (−71.2)	139.1 (146.8)	−173.09 (−179.9)
Arg	R	−105.2 (−61.9)	159.4 (156.5)	177.0 (179.8)
Gly	G	89.0 (−76.8)	38.4 (154.8)	–

Values in parentheses correspond to the original PDB structure.
[a] ϕ = C′-N-Cα-C′.
[b] ψ = N-Cα-C′-N.
[c] ω = Cα-C′-N-Cα.

Table 2B shows the time evolution of the number of HB between water molecules and PP residues, and Tables 3a and b show the time evolution of the number of HB between PC1 and water molecules during the MD production runs. In these last cases, the time step of analysis was of 500 ps, since the percentages of occupancy were smaller. By analyzing the results, it has been observed that there are no major changes in the number of water molecules that interact with the PP; just a small decrease is evidenced. The same occurs for the PC1 molecule. By comparing values of Tables 2B with 3a and b it is shown that PC1/water HB are stronger than those of PP/water, since the former exhibit higher occupancy percentages. Furthermore, PC1 forms more stable HB as an acceptor than as a donor, while it forms a greater number of HB as a donor than as an acceptor. The very low occupancy values, without a defined trend, indicate there is a constant renewal of the water molecules hydrogen-bonded to the analyzed carbonyls. This is expected if we consider that the system is highly diluted with a large number of water molecules.

The interatomic O···O distances of the three most stable interactions of Table 2A, that is, those with the highest percentages of occupancy were calculated as a function of the simulation time and they were plotted in Fig. 6. In accord with a stable donor-acceptor distance of a HB [60], after 5 ns of big fluctuations of these distances, PC1 binds to the PP through the O_{3F}–H···O_{LYS2} HB that lasts a few nanoseconds before breaking it. Throughout the trajectory the O_{3F}–H···O_{LYS2} HB and O_{5A}–H···O_{PRO3} (see Table 2A) are formed simultaneously, while O atoms of O_{7D}–H···O_{PRO5} HB are far apart to form a stable HB. Fig. 6 also shows that HB are interchanged (green plot with black and red) along all the simulation. Another interesting point is that the HB corresponding to the red line has more fluctuation than the rest of HB, which indicates a less stable bond.

Table 2A
Time evolution[a] of the percentages of occupancy of hydrogen bonds between the protein and PC1.

Time frame[b]	O_{5A}–H···O_{Lys2}	O_{7D}–H···O_{Lys2}	O_{3F}–H···O_{Lys2}	O_{3F}–H···O_{Gly1}	O_{7D}–H···O_{Pro5}	O_{5A}–H···O_{Pro3}
5	14.04	10.08	–	–	–	–
10	14.92	–	50.68	21.62	17.08	14.94
15	–	–	86.52	–	–	31.28
20	–	–	92.06	–	–	25.24
25	–	–	87.00	–	–	23.00
30	–	–	19.14	–	85.36	75.96
35	–	–	65.12	–	32.84	46.64
40	33.36	–	21.70	65.58	44.32	–
45	25.70	–	32.20	61.44	–	–
50	–	–	79.74	–	–	36.94
20	–	–	92.06	–	–	25.24

[a] Analysis time step in every time frame: 500 ps.

[b] In nanoseconds.

Table 2B
Time evolution[a] of the number of hydrogen bonds between water molecules and PP. residues, with percentages of occupancy ≥0%, ≥2%, ≥5%, and ≥ 10%.

Time frame[b]	≥0%	≥2%	≥5%	≥10%
5	750	90	17	2
10	736	104	13	1
15	706	119	10	1
20	752	113	13	1
25	612	87	14	2
30	862	105	11	0
35	796	91	13	1
40	631	89	16	1
45	604	104	15	5
50	607	97	21	3

[a] Analysis time step in every time frame: 500 ps.

[b] In nanoseconds.

Table 3
Time evolution[a] of the number of hydrogen bonds between water molecules and PC1 with percentages of occupancy ≥0%, ≥5%, ≥10% and ≥ 20%.

Time frame[b]	≥0%	≥5%	≥10%	≥20%
(a) PC1 as hydrogen-bond acceptor				
5	453	44	13	2
10	411	40	14	2
15	412	32	15	4
20	415	43	14	2
25	422	34	19	2
30	396	36	16	1
35	382	37	24	0
40	402	48	14	4
45	439	37	12	5
50	380	36	19	5
(b) PC1 as hydrogen-bond donor				
5	1551	6	0	0
10	1511	2	2	1
15	1452	5	1	0
20	1491	7	1	1
25	1449	9	1	0
30	1470	7	0	1
35	1492	8	2	0
40	1449	9	0	0
45	1533	7	1	0
50	1459	7	1	0

[a] Analysis time step in every time frame: 500 ps.

[b] In nanoseconds.

Finally, it can be seen that the HB denoted by a green line (O_{7D}–H···O_{PRO5}) oscillates between two main distances: 2.5 Å (distance corresponding to a stable HB) and 6.25 Å, which is a difference of 3.75 Å. This means that the PC1 and the PP change conformationally causing this elongation of the distance, as shown in Fig. 3b.

3.2. Topology of the electron density

The geometrical description of HB is not sufficient to establish the presence of an interaction. Since the Bader's QTAIM [35] unequivocally defines a chemical bonding by a bond path between two nuclei [61], this method is a powerful tool that has been successfully applied in the study of electronic properties of a variety of conventional and non-conventional HB [35,62–64], Therefore, to get a better understanding of the interactions involved, we applied this methodology over a structure taken from the MD simulation.

Structure of Fig. 5 was used to generate a wave function at the HF/6-31G(d) level of theory. Table 4 reports the most studied local topological properties calculated at BCP, and some approaches of the molecular graph of the complex are displayed in Figs. 7 and 9. Because of the size of the structure, BCP of covalent bonds were omitted for a better graphical understanding.

The topological analyses reveal the occurrence of several closed shell interactions. There are more non-conventional interactions involved than conventional ones. Values of electron density at BCPs lie in the order of HB criteria (0.002 to 0.034 a.u.) proposed by Koch and Popelier [62]; however, there are three interactions that are below 0.002 au. Values of Laplacian range from 0.05 to 0.1 which are in concordance with the values reported for similar interactions [62,64,65], In addition, the kinetic energy contribution is greater than that of the potential energy at the BCP, resulting in positive values of the total energy density. The presence of several close contacts like O···O, N···O and O···C should also be mentioned.

Stacking interactions between Pro residues and aromatic rings have been previously observed [32,33]. They were reported as face-to-face contacts between a polyphenolic ring and a Pro ring. They have also been referred to in the literature as hydrophobic interactions [66], although this term is not well defined. Experimental evidence of these interactions have also been reported [67]. In Fig. 7 (insets **a** and **b**), stacking interactions are clearly observed. This Figure also shows how the procyanidin seems to "hug" the protein with its phenolic rings. In Fig. 7a this hydrophobic interaction results in terms of HBs C—H···π type, that is C_{β}–H···C_{6A} (ρ = 0.0043 a.u.), C_{δ}–H···C_{5A} (ρ = 0.0037 a.u.) and C_{γ}–H···π (ρ = 0.0037 a.u.). In these interactions the bridge atom, H donor from Pro ring, is engaged to each carbon atom in the benzenic ring, except the last one in which the bond path is curved in the vicinity of the π-cloud but directed to the C atom. The same pattern is observed in Fig. 7b, in which the interactions are the following: C_{α}–H···π (ρ = 0.0059

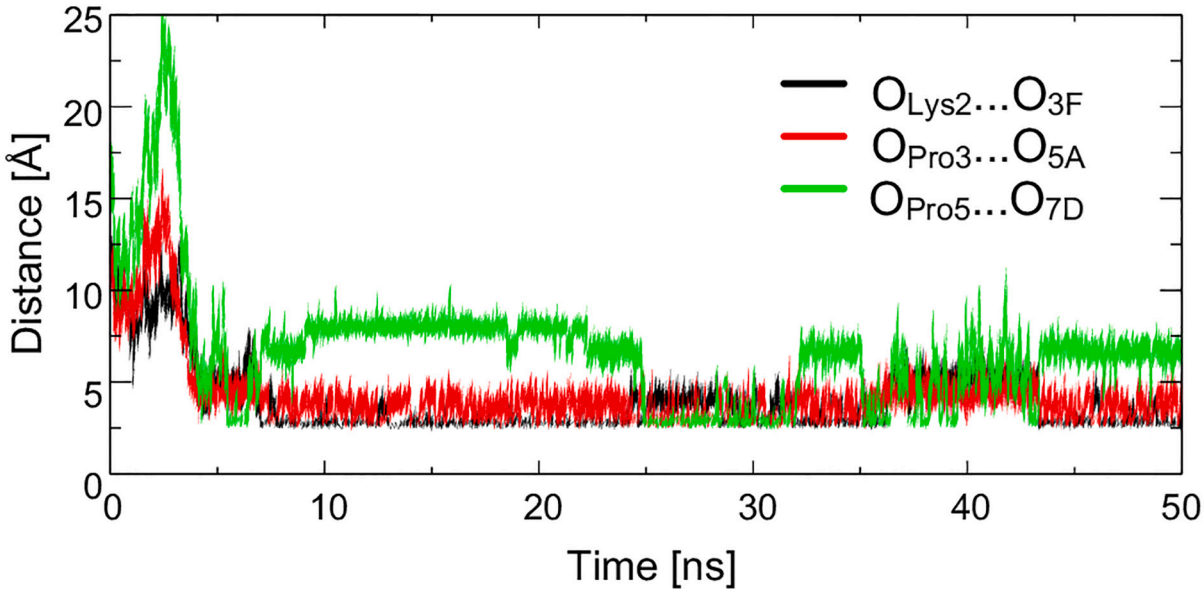

Fig. 6. Interatomic distances between O atoms, involved in HB, as a function of the simulation time.

Table 4
Local properties (in a.u.) at bond critical points in the complex protein/PC1caption.

Interaction	$\rho(r_c)$	$\nabla^2\rho(r_c)$	$V(r_c)$	$H(r_c)$
O_{5A}–H···O_{Pro3}	0.0001	0.0008	0.0000	0.0001
$C_{3'H}$ —H···O_{Gly1}	0.0011	0.0055	−0.0005	0.0005
C_{4F} —H···N_{Gly4}	0.0012	0.0055	−0.0006	0.0004
O_{1I}…O_{Lys2}	0.0029	0.0163	−0.0024	0.0008
$C_{\delta Pro5}$–H···C_{5A}	0.0037	0.0121	−0.0017	0.0007
$C_{\gamma Pro5}$–H···C_{6A}	0.0037	0.0129	−0.0019	0.0007
$C_{\gamma Pro5}$–H···O_{7D}	0.0040	0.0173	−0.0026	0.0009
$C_{\beta Pro5}$–H···C_{6A}	0.0043	0.0133	−0.0020	0.0006
$C_{\alpha Gly1}$–H···O_{3F}	0.0046	0.0204	−0.0030	0.0011
N_{Lys2}···O_{3F}	0.0049	0.0213	−0.0035	0.0009
$C_{\alpha Gly1}$–H···2CE·	0.0051	0.0174	−0.0025	0.0009
$C_{\alpha Pro3}$–H···$C_{1'H}$	0.0059	0.0206	−0.0032	0.0010
C_{4F}–H···O_{Lys2}	0.0061	0.0248	−0.0041	0.0010
$C_{\beta PRO3}$–H···$C_{5'H}$	0.0070	0.0251	−0.0040	0.0011
N_{Lys2}–H···$C_{1'E}$	0.0070	0.0247	−0.0040	0.0011
$C_{\beta Lys2}$–H···$C_{6'E}$	0.0088	0.0255	−0.0045	0.0009
O_{Lys2}···$C_{2'H}$	0.0090	0.0306	−0.0062	0.0007
$C_{\alpha Gly4}$–H···C_{5D}	0.0095	0.0352	−0.0057	0.0016
$C_{\alpha Gly4}$–H···O_{5D}	0.0096	0.0382	−0.0072	0.0012
$C_{\delta Pro5}$–H···C_{6D}	0.0110	0.0378	−0.0065	0.0015
O_{3F}–H···O_{Lys2}	0.0210	0.0799	−0.0198	0.0001

au) and C_{β}–H···$C_{5'H}$ (ρ = 0.0070 au).

In order to find out whether these stacking interactions are system- and/or method-dependent, we employed reduced systems based on the PC1/PP complex and optimized them at the BLYP-D3(BJ)/6–311++G(d,p) level of theory, as shown in Fig. 8. If we compare the insets of Fig. 7 with Figs. 8a and b, we can verify that the same C atoms of Pro are involved in the stacking interactions: C_{α}, C_{β} and C_{δ}. Since the interaction energies are equal for both systems, and they show the same BCP, the peptide-like bonds do not influence in the stacking. Values of electron density at these BCP lie in the order of HB criteria (0.002 to 0.034 a.u.) proposed by Koch and Popelier [62]. Moreover, ρ values of BCP displayed in Fig. 7b are almost equal to those obtained in Fig. 8 with a more rigorous level of theory (see Table S1 in supporting information). Summing up, there are three key interactions in the stacking phenomenon: C_{α}–H···$C_{4'}$, C_{δ}–H···$C_{6'}$, C_{β}–H···$C_{3'}$. Since the other BCP show ellipticity (ε) values that range from 1 to 17 (see Table S1 in supporting information), they are generally considered as labile or to be associated

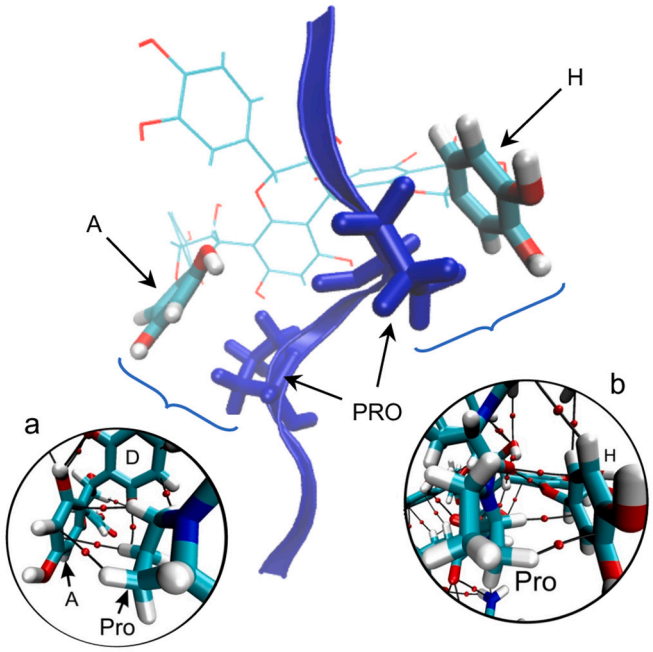

Fig. 7. PC1/PP complex showing the stacking interactions. The protein backbone is represented by ribbon model; proline residues and A and H PC1 rings are represented by liquorice model (a) Stacking interaction between ring A of PC1 and Pro ring. (b) Stacking interaction between ring H of PC1 and Pro ring.

with a tendency to break [63].

Another situation is shown in Fig. 9a, in which the O_{3F}–H···O_{LYS2} interaction, which was found in the MD simulation, is observed with a value of ρ = 0.021 au (see also the Supporting Discussion 1 in the supporting information). The multi-center interactions that the carbonyl oxygen of Lys can form: O_{3F}–H···O_{LYS2}, C_{4F}–H···O_{LYS} (ρ = 0.0061 a.u.) and a non-conventional interaction O_{LYS}···O_{1I}, which was observed in other biological systems [65,68] should be pointed out. Besides, the oxygen O_{3F} is hydrogen bonded to N—H bond from Lys. This interaction should be highlighted since, up to now, it has not been considered in the model description of the phenomenon of protein-polyphenol

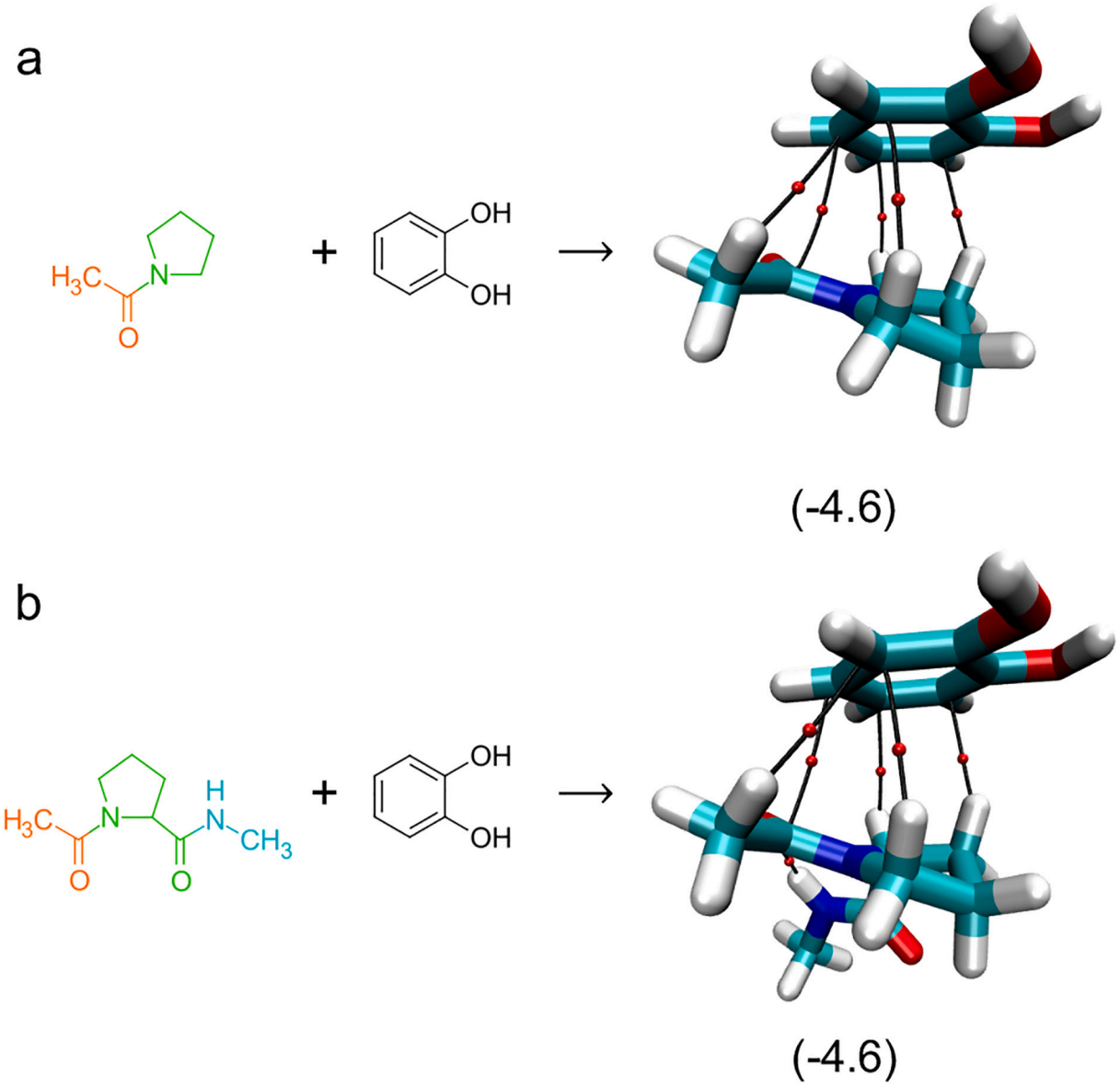

Fig. 8. (a) Molecular interactions between a pyrrolidine ring with a peptide-like bond and benzenediol. (b) Molecular interactions between a pyrrolidine ring with two peptide-like bonds and benzenediol. Interaction energies are shown in parentheses (in kcal mol^{-1}).

interaction. Also, if we consider the C═O bond of Lys2 attached to Pro3, some authors have argued that the carbonyl groups preceding Pro residues are more electronegative and therefore they have more tendency to form strong hydrogen bonds. [69–71] A more in-depth discussion of this hypothesis is given in Supporting Discussion 1 (Supporting Information).

Finally, in Fig. 9b the HB O_{5A}–H···O_{PRO3} is observed, whose value of ρ at BCP (0.0001 a.u.) is very low due to the wide interatomic O···O distance. This is in line with the analysis of Fig. 6, in which the interchange of HB is evidenced. Regarding the level of theory implemented to calculate the wave function, if we applied a higher level to compute it, the BCP could disappear. However, this topological analysis was shown to be sufficiently useful to describe the interactions at a molecular level.

4. Conclusions

In this paper, we have presented an extensive description of protein/polyphenol interactions at a molecular level between the Procyanidin C1 and a collagen-like peptide. The most significant result of this work is the spontaneous formation of a stable complex led by O—H···O and C—H···π hydrogen bonds, being the latter previously called *stacking interaction*.

The QTAIM results show a wide scene of contributions that are relevant to the stabilization of the complex. It is clear that the main interaction that binds the compounds is the typical O—H···O hydrogen bond, between an –OH phenol group and a carbonyl oxygen from the peptide bond. Because the PC1 is not in a fixed position of the PP, the stacking interactions play a key role to stabilize the complex and to assist to its dynamic motion. The polyphenol moves between two main aminoacids, which are Lys and Pro. The analysis of interaction sites confirms that the PC1 prefers Pro residues, as it has already been mentioned in the literature. Therefore, Pro residues not only promote the opening of the structures by leaving the C═O groups available, but also, they serve as a platform for stacking interactions. The PGP sequence, which can also be found in $(PPG)_n$ motifs, is a key factor for the bonding mechanism because it provides the platform for stacking interactions and hydrogen bonding sites near the Pro residues.

The current study has also found that the polyphenol affects the

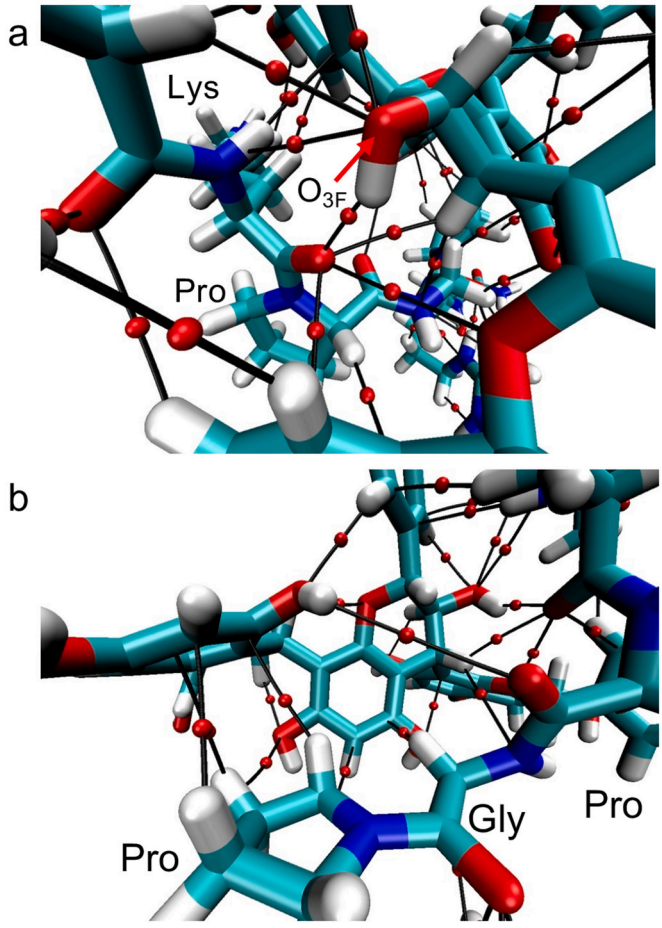

Fig. 9. Molecular graphs close ups of the PC1/PP complex. (a) Molecular interactions involving O_{Lys2}. The O_{3F}–H···O_{Lys2} HB is also shown. (b) Close up showing the O_{5A}–H···O_{Pro3} interaction.

conformation of the PP. Major fluctuations of PP backbone occur in aqueous solution, while in the presence of the PC1 they decrease drastically where the polyphenol is bonded.

All of these findings open up a new insight into the polyphenol/protein interactions which have not been previously explored, providing a better understanding of the phenomena like colloidal turbidity, astringency, tanning and the secondary effects of flavonoid compounds in enzymatic systems.

Declaration of Competing Interest

The authors declare that they have no known competing financial interests or personal relationships that could have appeared to influence the work reported in this paper.

Data availability

Data will be made available on request.

Acknowledgements

The authors gratefully acknowledge the financial support from the Secretaría de Ciencia y Tecnología, Universidad Tecnológica Nacional, Facultad Regional Resistencia (SCYT-UTN-FRRe). A.N.P. thanks the National Scientific and Technical Research Council (CONICET), Argentina, for a postdoctoral fellowship. The authors also gratefully thank AMBER developers for donating the AMBER 11 software.

Appendix A. Supplementary data

Supplementary data to this article can be found online at https://doi.org/10.1016/j.bpc.2021.106627.

References

[1] C.G. Fraga, M. Galleano, S.V. Verstraeten, P.I. Oteiza, Basic biochemical mechanisms behind the health benefits of polyphenols, Mol. Asp. Med. 31 (2010) 435–445.
[2] G.R. Scollary, G. Pásti, M. Kállay, J. Blackman, A.C. Clark, Astringency response of red wines: potential role of molecular assembly, Trends Food Sci. Technol. 27 (2012) 25–36.
[3] E. Steiner, T. Becker, M. Gastl, J.I. Brew, Turbidity and haze formation in beer – insights and overview, J. Inst. Brew. 116 (2010) 360–368.
[4] C.T. Ho, Q.Y. Chen, H. Shi, K.-Q. Zhang, R.T. Rosen, Antioxidant effect of polyphenol extract prepared from various Chinese teas, Prev. Med. 21 (1992) 520–525.
[5] Z.P. Xue, W.H. Feng, J.K. Cao, D.D. Cao, W.B. Jiang, Antioxidant activity and total phenolic contents in peel and pulp of chinese jujube (ziziphus jujuba mill) fruits, J. Food Biochem. 33 (2009) 613–629.
[6] T. Hirano, M. Gotoh, K. Oka, Citrus flavone tangeretin inhibits leukaemic HL-60 cell growth partially through induction of apoptosis with less cytotoxicity on normal lymphocytes, Life Sci. 55 (1994) 1061–1069.
[7] J.N. Davis, O. Kucuk, F.H. Sarkar, Genistein inhibits NF-κB activation in prostate cancer cells, Nutr. Cancer 35 (1999) 167–174.
[8] R. Huet, Constituents of citrus fruits with pharmacodynamic effect: citroflavonoids, Fruits. 37 (1982) 267–271.
[9] H. Akiyama, J. Sakushima, S. Taniuchi, T. Kanda, A. Yanagida, T. Kojima, R. Teshima, Y. Kobayashi, Y. Goda, M. Toyoda, Antiallergic effect of apple polyphenols on the allergic model mouse, Biol. Pharm. Bull. 23 (2000) 1370–1373.
[10] G.L. Tipoe, T.M. Leung, M.W. Hung, M.L. Fung, Green tea polyphenols as an anti-oxidant and anti-inflammatory agent for cardiovascular protection, Cardiovasc. Hematol. Disord. Drug Targets. 7 (2007) 135–144.
[11] E.M. Galati, M.T. Monforte, S. Kirjavainen, A.M. Forestieri, A. Trovato, M. M. Tripodo, Biological effects of hesperidin, a citrus flavonoid. (Note I): antiinflammatory and analgesic activity, Farmaco 40 (1994) 709–712.
[12] L. Chapon, Points of interest concerning the chill haze of beer, Brauwelt. 108 (1968) 1769–1775.
[13] K.J. Siebert, Haze formation in beverages, LWT Food Sci. Technol. 39 (2006) 987–994.
[14] S. Tajchakavit, J.I. Boye, D. Bélanger, R. Couture, Kinetics of haze formation and factors influencing the development of haze in clarified apple juice, Food Res. Int. 34 (2001) 431–440.
[15] R. Ben Abdallah, A.B. Bautista-Ortin, T. Ghazouani, W. Talbi, M.D. Jiménez-Martinez, E. Gómez-Plaza, S. Fattouch, Proteolytic regulation of the extent of dietary proteins with skin grape proanthocyanidin and anthocyanidin's interactions, Int. J. Food Sci. Technol. 54 (2019) 1633–1641.
[16] K.J. Siebert, N.V. Troukhanova, P.Y. Lynn, Nature of polyphenol-protein interactions, J. Agric. Food Chem. 44 (1996) 80–85.
[17] H.I. Oh, J.E. Hoff, G.S. Armstrong, L.A. Haff, Hydrophobic interaction in tanning-protein complexes, J. Agric. Food Chem. 28 (1980) 394–398.
[18] A.N. Petelski, S.C. Pamies, E.I. Benítez, M.M.L. Rovaletti, G.L. Sosa, Molecular insights into protein-polyphenols aggregation: a dynamic and topological description, ChemistrySelect. 2 (2017) 5608–5615.
[19] A.E. Hagerman, L.G. Butler, The specificity of proanthocyanidin-protein interactions, J. Biol. Chem. 256 (1981) 4494–4497.
[20] K. Asano, K. Shinagawa, N. Hashimoto, Characterization of haze-forming proteins of beer and their roles in chill haze formation, J. Am. Soc. Brew. Chem. 40 (1982) 147–154.
[21] R. Sutherland, Tanning industry, Ind. Eng. Chem. 39 (1947) 628–631.
[22] G.D. McLaughlin, F. O'Flaherty, The technology of tanning, J. Chem. Educ. 6 (1929) 1019–1034.
[23] S. Bronco, C. Cappelli, S. Monti, Understanding the structural and binding properties of collagen: a theoretical perspective, J. Phys. Chem. B 108 (2004) 10101–10112.
[24] S. Monti, S. Bronco, C. Cappelli, Toward the supramolecular structure of collagen: a molecular dynamics approach, J. Phys. Chem. B 109 (2005) 11389–11398.
[25] G.J. McDougall, D. Stewart, The inhibitory effects of berry polyphenols on digestive enzymes, BioFactors. 23 (2005) 189–195.
[26] Y. Kimura, H. Ito, R. Ohnishi, T. Hatano, Inhibitory effects of polyphenols on human cytochrome P450 3A4 and 2C9 activity, Food Chem. Toxicol. 48 (2010) 429–435.
[27] M. Mozzicafreddo, M. Cuccioloni, V. Cecarini, A.M. Eleuteri, M. Angeletti, Homology modeling and docking analysis of the interaction between polyphenols and mammalian 20S proteasomes, J. Chem. Inf. Model. 49 (2009) 401–409.
[28] N.F. Brás, R. Gonçalves, N. Mateus, P.A. Fernandes, M.J. Ramos, V. de Freitas, Inhibition of pancreatic elastase by polyphenolic compounds, J. Agric. Food Chem. 58 (2010) 10668–10676.
[29] B.G. Green, Oral astringency: a tactile component of flavor, Acta Psychol. 84 (1993) 119–125.
[30] E. Haslam, M.P. Williamson, N.J. Baxter, A.J. Charlton, Astringency and protein polyphenol interactions, Recent Adv. Phytochem. 33 (1999) 289–318.

[31] E. Jöbstl, J. O'Connell, J.P.A. Fairclough, M.P. Williamson, Molecular model for astringency produced by polyphenol/protein interactions, Biomacromolecules 5 (2004) 942–949.
[32] N.J. Baxter, T.H. Lilley, E. Haslam, M.P. Williamson, Multiple interactions between polyphenols and a salivary proline-rich protein repeat result in complexation and precipitation, Biochemistry. 2960 (1997) 5566–5577.
[33] A.J. Charlton, E. Haslam, M.P. Williamson, Multiple conformations of the proline-rich protein/epigallocatechin gallate complex determined by time-averaged nuclear overhauser effects, J. Am. Chem. Soc. 124 (2002) 9899–9905.
[34] C. Simon, K. Barathieu, M. Laguerre, J. Schmitter, E. Fouquet, I. Pianet, E. J. Dufourc, Three-dimensional structure and dynamics of wine tannin - saliva protein complexes a multitechnique approach, Biochemistry. 42 (2003) 10385–10395.
[35] R.F.W. Bader, Atoms in Molecules: A Quantum Theory, Clarendon Press, Oxford, 1994.
[36] S. De Pascual-Teresa, C. Santos-Buelga, J.C. Rivas-Gonzalo, Quantitative analysis of flavan-3-ols in spanish foodstuffs and beverages, J. Agric. Food Chem. 48 (2000) 5331–5337.
[37] F. Saura-Calixto, J. Serrano, J. Pérez-Jiménez, What contribution is beer to the intake of antioxidants in the diet? in: V.R. Preedy (Ed.), Beer in Health and Disease Prevention Academic Press, San Diego, 2009, pp. 441–448.
[38] M.J. Frisch, G.W. Trucks, H.B. Schlegel, G.E. Scuseria, M.A. Robb, J.R. Cheeseman, G. Scalmani, V. Barone, B. Mennucci, G.A. Petersson, H. Nakatsuji, M. Caricato, X. Li, H.P. Hratchian, A.F. Izmaylov, J. Bloino, G. Zheng, J.L. Sonnenberg, M. Hada, M. Ehara, K. Toyota, R. Fukuda, J. Hasegawa, M. Ishida, T. Nakajima, Y. Honda, O. Kitao, H. Nakai, T. Vreven, J.A. Montgomery Jr., J.E. Peralta, F. Ogliaro, M. Bearpark, J.J. Heyd, E. Brothers, K.N. Kudin, V.N. Staroverov, T. Keith, R. Kobayashi, J. Normand, K. Raghavachari, A. Rendell, J.C. Burant, S.S. Iyengar, J. Tomasi, M. Cossi, N. Rega, J.M. Millam, M. Klene, J.E. Knox, J.B. Cross, V. Bakken, C. Adamo, J. Jaramillo, R. Gomperts, R.E. Stratmann, O. Yazyev, A. J. Austin, R. Cammi, C. Pomelli, J.W. Ochterski, R.L. Martin, K. Morokuma, V. G. Zakrzewski, G.A. Voth, P. Salvador, J.J. Dannenberg, S. Dapprich, A.D. Daniels, O. Farkas, J.B. Foresman, J.V. Ortiz, J. Cioslowski, D.J. Fox, Gaussian 09, Revision D.01, Gaussian, Inc., Wallingford CT, 2013.
[39] C.I. Bayly, P. Cieplak, W.D. Cornell, P.A. Kollman, Well-behaved electrostatic potential based method using charge restraints for deriving atomic charges: the RESP model, J. Phys. Chem. 97 (1993) 10269–10280.
[40] F. Delacoux, A. Fichard, C. Geourjon, R. Garrone, F. Ruggiero, Molecular features of the collagen V heparin binding site, J. Biol. Chem. 273 (1998) 15069–15076.
[41] M.D. Shoulders, R.T. Raines, Collagen structure and stability, Annu. Rev. Biochem. 78 (2009) 929–958.
[42] V. Gauba, J.D. Hartgerink, Self-assembled heterotrimeric collagen triple helices directed through electrostatic interactions, J. Am. Chem. Soc. 129 (2007) 2683–2690.
[43] J.W. Smith, Molecular pattern in native collagen, Nature. 219 (1968) 157–158.
[44] W.L. Jorgensen, Transferable intermolecular potential functions for water, alcohols, and ethers. Application to liquid water, J. Am. Chem. Soc. 103 (1981) 335–350.
[45] D.A. Case, K. Belfon, I.Y. Ben-Shalom, S.R. Brozell, D.S. Cerutti, T.E. Cheatham III, V.W.D. Cruzeiro, T.A. Darden, R.E. Duke, G. Giambasu, M.K. Gilson, H. Gohlke, A. W. Goetz, R. Harris, S. Izadi, S.A. Izmailov, K. Kasavajhala, A. Kovalenko, R. Krasny, T. Kurtzman, T.S. Lee, S. LeGrand, P. Li, C. Lin, J. Liu, T. Luchko, R. Luo, V. Man, K.M. Merz, Y. Miao, O. Mikhailovskii, G. Monard, H. Nguyen, A. Onufriev, F. Pan, S. Pantano, R. Qi, D.R. Roe, A. Roitberg, C. Sagui, S. Schott-Verdugo, J. Shen, C. Simmerling, N.R. Skrynnikov, J. Smith, J. Swails, R.C. Walker, J. Wang, L. Wilson, R.M. Wolf, X. Wu, Y. Xiong, Y. Xue, D.M. York, P.A. Kollman, AMBER 11, University of California, San Francisco, 2010.
[46] J.A. Izaguirre, D.P. Catarello, J.M. Wozniak, R.D. Skeel, Langevin stabilization of molecular dynamics, J. Chem. Phys. 114 (2001) 2090–2098.
[47] J.P. Ryckaert, G. Ciccotti, H.J. Berendsen, Numerical-integration of cartesian equations of motion of a system with constraints - molecular-dynamics of n-alkanes, J. Comput. Phys. 23 (1977) 327–341.
[48] T.A. Keith, AIMAll (Version 12.06.03), T.K. Gristmill Software, Overland Park KS, USA, 2012.
[49] T. Lu, F. Chen, Multiwfn: a multifunctional wavefunction analyzer, J. Comput. Chem. 33 (2012) 580–592.
[50] E. Espinosa, E. Molins, C. Lecomte, Hydrogen bond strengths revealed by topological analyses of experimentally observed electron densities, Chem. Phys. Lett. 285 (1998) 170–173.
[51] W. Humphrey, A. Dalke, K. Schulten, VMD - Visual molecular dynamics, J. Mol. Graph. 14 (1996) 33–38.
[52] A.D. Becke, Density-functional exchange-energy approximation with correct asymptotic behavior, Phys. Rev. A 38 (1988) 3098–3100.
[53] C. Lee, W. Yang, R.G. Parr, Development of the colle-salvetti correlation-energy formula into a functional of the electron density, Phys. Rev. B 37 (1988) 785–789.
[54] S. Grimme, J. Antony, S. Ehrlich, H. Krieg, A consistent and accurate ab initio parametrization of density functional dispersion correction (DFT-D) for the 94 elements H-Pu, J. Chem. Phys. 132 (2010) 154104.
[55] E.R. Johnson, A.D. Becke, A post-Hartree–Fock model of intermolecular interactions, J. Chem. Phys. 123 (2005), 024101.
[56] M.T. Carroll, R.F.W. Bader, An analysis of the hydrogen bond in BASE-HF complexes using the theory of atoms in molecules, Mol. Phys. 65 (1988) 695–722.
[57] D. Cremer, E. Kraka, Chemical bonds without bonding electron density – does the difference electron-density analysis suffice for a description of the chemical bond? Angew. Chem. Int. Ed. 23 (1984) 627–628.
[58] B. Bochicchio, A.M. Tamburro, Polyproline II structure in proteins: identification by chiroptical spectroscopies, stability, and functions, Chirality. 14 (2002) 782–792.
[59] G.R. Desiraju, T. Steiner, The Weak Hydrogen Bond: In Structural Chemistry and Biology, Oxford University Press, 2001.
[60] T. Steiner, Unrolling the hydrogen bond properties of C–H···O interactions, Chem. Commun. (1997) 727–734.
[61] R.F.W. Bader, A bond path: a universal indicator of bonded interactions, J. Phys. Chem. A 102 (1998) 7314–7323.
[62] U. Koch, P.L.A. Popelier, Characterization of C-H-O hydrogen bonds on the basis of the charge density, J. Phys. Chem. 99 (1995) 9747–9754.
[63] P.L.A. Popelier, Characterization of a dihydrogen bond on the basis of the electron density, J. Phys. Chem. A 102 (1998) 1873–1878.
[64] N.J.M. Amezaga, S.C. Pamies, N.M. Peruchena, G.L. Sosa, Halogen bonding: a study based on the electronic charge density, J. Phys. Chem. A 114 (2010) 552–562.
[65] S.A. Andujar, R.D. Tosso, F.D. Suvire, E. Angelina, N. Peruchena, N. Cabedo, D. Cortes, R.D. Enriz, Searching the "biologically relevant" conformation of dopamine: a computational approach, J. Chem. Inf. Model. 52 (2012) 99–112.
[66] A.E. Hogerman, Fifty years of polyphenol-protein complexes, in: V. Cheynier, P. Sarni-Manchado, S. Quideau (Eds.), Recent Advances in Polyphenol Research, John Wiley & Sons, 2012, pp. 79–80.
[67] N.J. Murray, M.P. Williamson, T.H. Lilley, E. Haslam, Study of the interaction between salivary proline-rich proteins and a polyphenol by 1H NMR spectroscopy, Eur. J. Biochem. 219 (1994) 923–935.
[68] E.L. Angelina, S.A. Andujar, R.D. Tosso, R.D. Enriz, N.M. Peruchena, Non-covalent interactions in receptor-ligand complexes. A study based on the electron charge density, J. Phys. Org. Chem. 27 (2014) 128–134.
[69] A. Veis, C.F. Nawrot, Basicity differences among peptide bonds, J. Am. Chem. Soc. 92 (1970) 3910–3914.
[70] K.A. Williams, C.M. Deber, Proline residues in transmembrane helices: structural or dynamic role? Biochemistry. 30 (1991) 8919–8923.
[71] C.M. Deber, B. Brodsky, A. Rath, Proline residues in proteins, in encycloped, Life Sci. (2010), https://doi.org/10.1002/9780470015902.a0003014.pub2.